IEEE Access
Multidisciplinary ⋮ Rapid Review ⋮ Open Access Journal

Received March 6, 2022, accepted March 28, 2022, date of publication March 31, 2022, date of current version April 7, 2022.

Digital Object Identifier 10.1109/ACCESS.2022.3163824

Novel Hybrid Consequent-Pole Brushless Wound Rotor Synchronous Machine for Improving Torque Characteristics

YING YAN[1], SYED SABIR HUSSAIN BUKHARI[2], (Senior Member, IEEE), AND JONGSUK RO[1]

[1]School of Electrical and Electronics Engineering, Chung-Ang University, Seoul 06974, South Korea
[2]Department of Electrical Engineering, Sukkur IBA University, Sukkur, Sindh 65200, Pakistan

Corresponding author: Jongsuk Ro (jongsukro@gmail.com)

This work was supported in part by the Basic Science Research Program through the National Research Foundation of Korea funded by the Ministry of Education under Grant 2016R1D1A1B01008058; in part by the Brain Pool (BP) Program through the NRF of Korea funded by the Ministry of Science and ICT under Grant 2019H1D3A1A01102988; and in part by the Chung-Ang University Young Scientist Scholarship, in 2020.

ABSTRACT This article introduces a hybrid consequent-pole brushless wound rotor synchronous machine (CP-BL-WRSM). The CP-BL-WRSM installs permanent magnets (PMs) on the alternative rotor poles. Compared with the conventional BL-WRSM and permanent magnet-assisted brushless WRSM (PM-BL-WRSM), the proposed machine provides advantages of high average output torque, high maximum torque, and high starting torque. In addition, the proposed CP-BL-WRSM's torque ripple is also lower than the conventional brushless WRSM. The volume of PM in the CP-BL-WRSM machine is lower than the conventional permanent magnet synchronous machines (PMSMs) and PM-BL-WRSM. In this brushless topology, the machine uses three-phase stator windings powered by a single inverter, which provides a unique armature current to the stator windings that comprises of fundamental and third-harmonic components. The fundamental current component is used to generate the main stator field, and the third-harmonic current component is used to induce a harmonic current in the harmonic winding. A diode rectifier installed on the rotor is used to rectify the harmonic current. After the rectification, a direct current (DC) is injected into the field winding of the rotor to form a rotor magnetic field and achieve brushless operation. In order to verify the operation of the proposed CP-BL-WRSM topology and analyze its performance, 2-D finite element analysis (FEA) was used in JMAG-Designer. Finally, the performance of the proposed CP-BL-WRSM topology was compared with the conventional BL-WRSM topology and PM-BL-WRSM topology to verify its higher starting torque, higher average torque, and higher maximum torque and higher minimum torque. The proposed topology can replace the existing highly expensive PM synchronous machines (PMSMs) due to its less PM volume and conventional BL-WRSMs due to its better performance.

INDEX TERMS Brushless excitation, synchronous machine, consequent-pole, harmonic winding, 2-D finite element analysis (FEA).

I. INTRODUCTION

The PMSM has a wide range of applications because of its high power factor, and high efficiency. The PMSM uses PMs to provide excitation. Thus, this motor is independent of excitation current, with no excitation losses, simple structure, and improved efficiency. PMSMs eliminate problem-prone equipment such as brushes, slip rings, and additional exciters, which improve the reliability of the motor operation, reduce cost, reduce maintenance, and reduce motor size [1]–[4].

But in recent years, researchers are studying the replacement of PMSMs. Because the PM material used in the PMSM is based on rare earth metals with high magnetic energy product value, the price of this material is rising day by day, and the environmental pollution caused during the transportation cannot be ignored, so researchers are actively studying and developing other motors to replace PMSMs [5]–[7] for

The associate editor coordinating the review of this manuscript and approving it for publication was Akshay Kumar Saha.

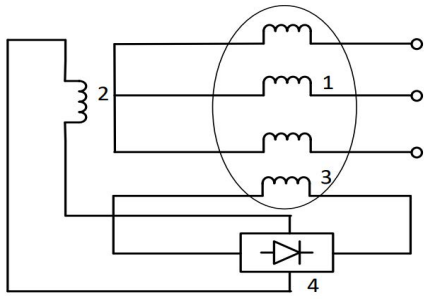

1. Main winding 2. Field winding
3. Harmonic winding 4. Rectifier

FIGURE 1. Schematic diagram of harmonic excitation of synchronous generator.

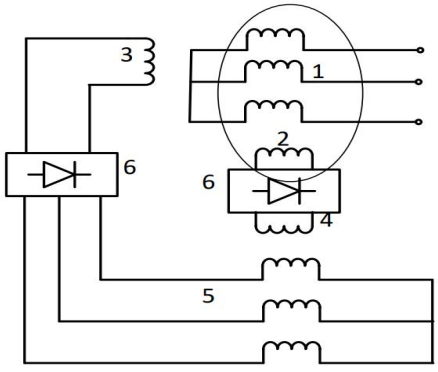

1. The generator main winding 2. The generator third winding
3. The generator field winding 4. The exciter field winding
5. The exciter armature winding 6. Rectifier

FIGURE 2. Existing brushless harmonically excited synchronous generator.

example, a wound rotor synchronous motor (WRSM) that does not require PM material.

WRSM has been studied in China in the last 40 years. Its working principle is to enhance the third-harmonic in the rotor magnetic field through the specially designed rotor magnetic pole shape. When the main magnetic field rotates, the third-harmonic back-EMF is induced in the harmonic winding, and the induced back-EMF passes through the rectifier, slip ring and the brushes are transferred to the rotor field winding, as shown in Fig. 1. In the above-mentioned WRSM, the generation of the rotor magnetic field requires problem-prone equipment such as brushes and slip rings, which can cause excessive losses, sparks, etc., and require regular maintenance, it will increase the motor cost. In order to eliminate the use of brushes and slip rings and reduce their adverse effects, Fig. 2 shows an additional exciter that assists the motor to achieve brushless harmonic excitation. However, the additional exciter also increases the size and cost of the motor, limiting its application in small and medium-sized motors [8]–[10].

In order to avoid the adverse effects of brushes, slip rings, and exciters in the conventional WRSM, the researchers proposed the BL-WRSM topologies [11]–[15]. The principle

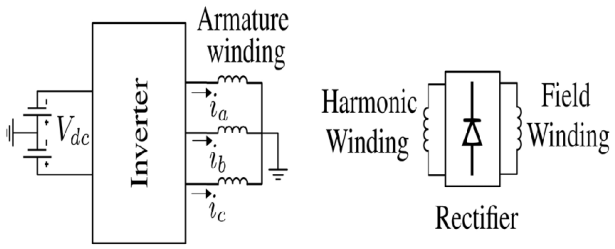

FIGURE 3. Illustration of the proposed brushless topology.

of these types of brushless topologies is mainly based on harmonic excitation technology. BL-WRSM has the characteristics of low cost as compared with PMSM [14], [16]–[18]. Therefore, the brushless operation of WRSM can make BL-WRSM a substitute of PMSM. The rotor of BL-WRSM is composed of the field winding, harmonic winding, and diode rectifier. The stator is composed of three-phase armature winding and field winding [19]–[21].

The starting torque of PMSM is higher than BL-WRSM. The low starting torque of BL-WRSM makes it unsuitable for variable speed applications. In order to make BL-WRSM suitable for variable speed applications, a PM-BL-WRSM is proposed in [22], [23]. The proposed hybrid BL-WRSM topology can increase the starting torque and the torque density of the motor under full load conditions. The difference between BL-WRSM and PM-BL-WRSM is the rotor structure. In the PM-BL-WRSM, PMs are inserted into the main teeth of the rotor. The stator winding configuration of PM-BL-WRSM is the same as that of BL-WRSM. However, inserting PMs into each pole of the rotor increases the cost of the PM-BL-WRSM topology.

Therefore, it is proposed in [24]–[27] that a consequent-pole permanent magnet motor uses fewer magnets to show similar performance compared with the conventional PM-BL-WRSM. As the volume of the magnet is reduced, so the cost of the motor is decreased. It is a cost-effective solution. In [26], a consequent-pole toroidal winding vernier permanent magnet (CP-TWVPM) machine was introduced. Facts have proved that the back-EMF and torque of this machine are about 20% higher than that of conventional VPM machines, while the number of magnets used is halved [24], [25]. However, in this topology, the sub-harmonic field excitation technique was used.

Because of the high performance of third-harmonic excitation technology, CP-BL-WRSM topology is proposed in this article to overcome the low starting torque issue and the large volume of PMs used in the third-harmonic based PM-assisted BL-WRSM. Fig. 3 shows the brushless topology proposed in this article. Compared with the BL-WRSM using dual-inverter configuration, this topology has the advantage of using a single inverter. A single inverter can effectively reduce the cost, weight, and size of the machine system compared to the dual-inverter configuration.

In this topology, the machine uses a three-phase stator winding powered by a single inverter. This inverter provides a

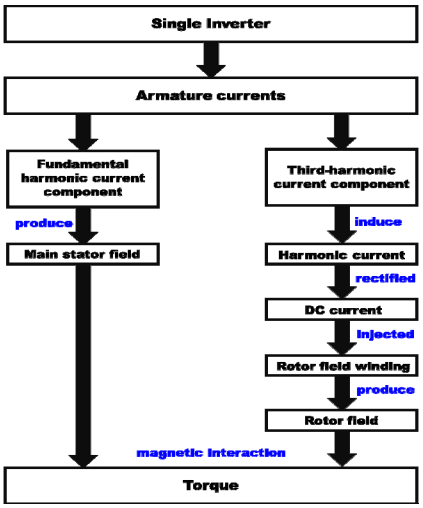

FIGURE 4. Brushless operation working principle.

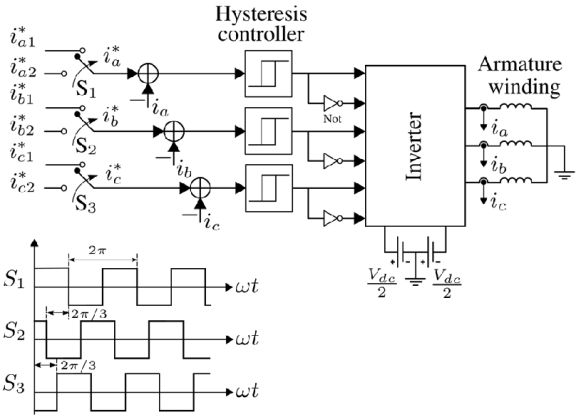

FIGURE 5. Detailed illustration of the proposed inverter topology.

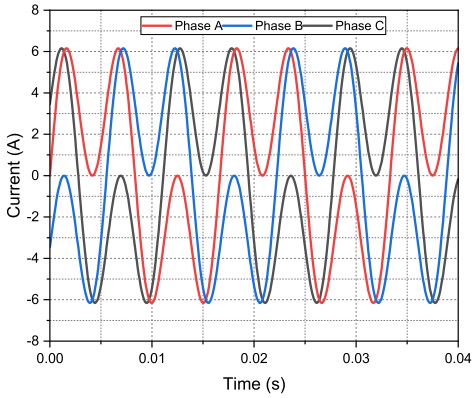

FIGURE 6. Three-phase output currents of the proposed inverter topology.

unique armature current to the stator winding that comprises of fundamental component and a third-harmonic component.

The main contributions of the research presented in this paper are as follows:

- A BL-WRSM topology based on the third-harmonic field excitation technique is used. This brushless topology employs a single inverter and a single stator armature winding configuration. Disadvantages of this topology are its low starting, average, maximum and minimum torques. These disadvantages are addressed by proposing a PM-BL-WRSM topology.
- A hybrid consequent-pole BL-WRSM topology based on the third-harmonic field excitation technique is proposed in this paper by using PMs on alternative rotor poles. This topology offers the advantages of high starting torque, high maximum torque, high average torque, and high minimum torque as compared to the PM-assisted BL-WRSM topology despite using a low volume of PMs which will make it cost-effective as well.
- The proposed hybrid CP-BL-WRSM could be a better candidate in the application where better torque characteristics are required as compared to the other BL-WRSM topologies employing harmonic field excitation techniques.

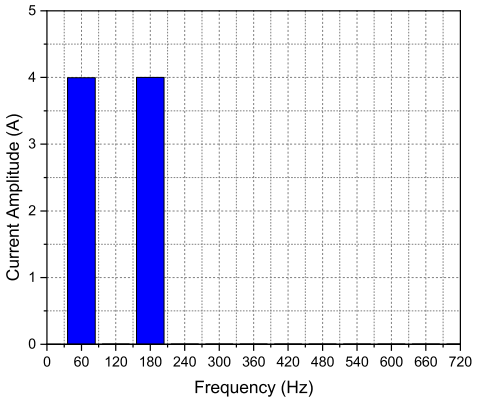

FIGURE 7. Inverter output currents FFT plot.

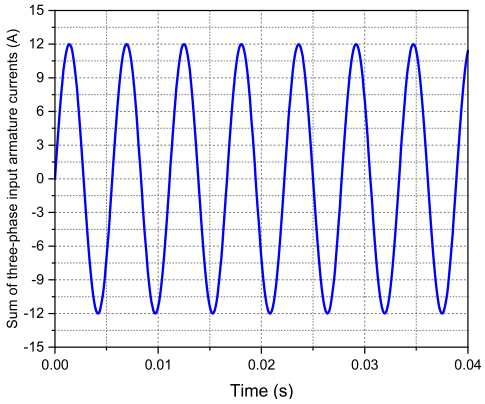

FIGURE 8. Sum of the three-phase input armature currents.

The operation of the three machine topologies were verified using 2-D FEA and the performance of CP-BL-WRSM with PM-BL-WRSM and BL-WRSM is compared. This article consists of the following sections:

Section 2 introduces the operating principle, section 3 describes the machine topologies, section 4 presents the performance analysis of three machines by 2-D FEA, and

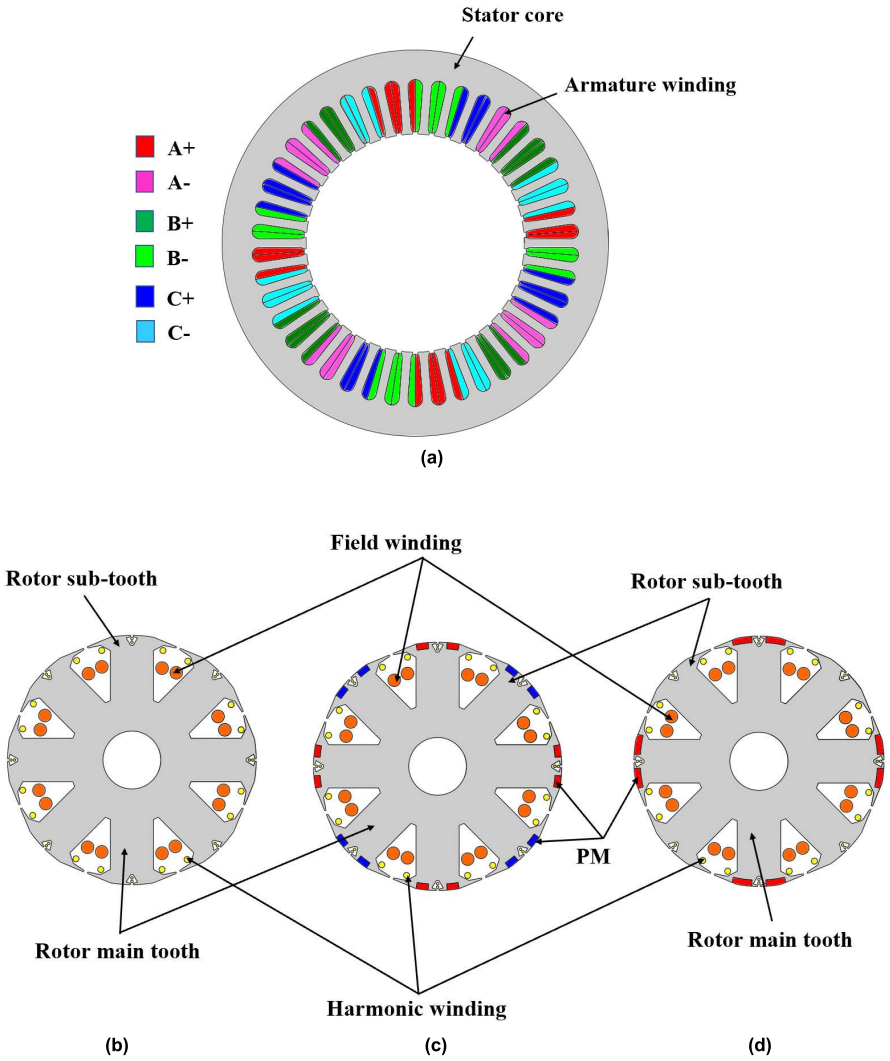

FIGURE 9. Machine topologies (a) Stator, and rotors for (b) conventional BL-WRSM, (c) PM-BL-WRSM, and (d) CP-BL-WRSM.

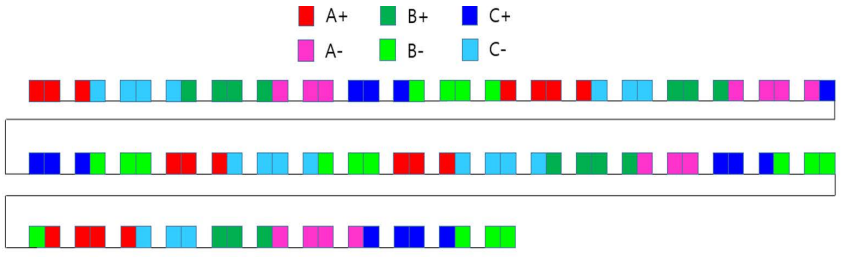

FIGURE 10. Stator winding pattern.

section 5 presents the conclusion of the research work proposed in this paper.

II. OPERATING PRINCIPLE OF SINGLE-INVERTER-CONTROLLED BL-WRSM TOPOLOGY

This paper uses a single inverter for the brushless operation of WRSM. The inverter adopts a simple current control scheme based on a hysteresis controller and provides input armature currents of unique shape. The frequency of the currents is set to 60 Hz and 180 Hz, and the input armature current's amplitude is 4 A. The composite armature current output by the inverter includes the fundamental component and the third-harmonic component. The fundamental component is used to generate the main stator field, and the third-harmonic component is used to induce harmonic current in

TABLE 1. Winding parameters for the employed machine.

Parameter	Value
Number of poles	8
Number of slots	42
Number of layers	2
Coil span	6 slots
Pole pitch	5.25 slots
Periodicities	2
Winding factor	0.932

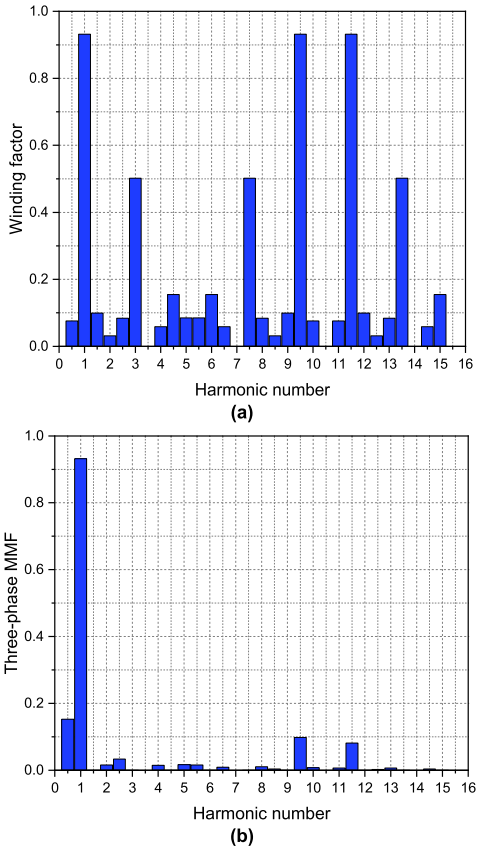

FIGURE 11. (a) Winding factors, (b) Three-phase MMF for different harmonic numbers generated for the employed stator windings.

the harmonic winding. A diode rectifier installed on the rotor is used to rectify the harmonic current. After the rectification is completed, a DC is injected into the field winding of the rotor to form a rotor magnetic field and achieve brushless operation. When the rotor magnetic field is generated, the torque will be generated as it cooperates with the stator magnetic field. The inverter topology is shown in Fig. 4, however, its detailed operation to achieve the required composite current shape is well-discussed in [6]. As shown in Fig. 5, the inverter uses a hysteresis current controller to develop an input armature current that contains two components, one of which is the fundamental component, and the other is the third-harmonic component. Therefore, the proposed topology requires the inverter to have two DC power supplies.

The controller of the inverter uses reference signals i_a^*, i_b^* and i_c^* generated using the following equation:

$$\begin{aligned} i_{a1}^* &= I_f \sin(\omega t) \\ i_{a2}^* &= I_t \sin 3(\omega t) \\ i_{b1}^* &= I_f \sin(\omega t - \frac{2\pi}{3}) \\ i_{b2}^* &= I_t \sin 3(\omega t - \frac{2\pi}{3}) \\ i_{c1}^* &= I_f \sin(\omega t + \frac{2\pi}{3}) \\ i_{c2}^* &= I_t \sin 3(\omega t + \frac{2\pi}{3}) \end{aligned} \tag{1}$$

Fig. 6 shows the three-phase output current of the inverter. Using fast Fourier transform (FFT) these currents are analyzed to show their harmonic content. Fig. 7 shows the FFT plot of the input armature currents for *A*-phase. This plot shows that the inverter output current contains two current components, the third-harmonic component, and the fundamental current component. The sum of the three-phase armature currents, which is input from the proposed inverter, produces the third-harmonic waveform as shown in Fig. 8.

The three-phase input armature currents are shown in (2).

$$\left.\begin{aligned} i_a(t) &= I_f \sin(\omega t) + I_t \sin 3(\omega t) \\ i_b(t) &= I_f \sin(\omega t - \tfrac{2\pi}{3}) + I_t \sin 3(\omega t - \tfrac{2\pi}{3}) \\ i_c(t) &= I_f \sin(\omega t + \tfrac{2\pi}{3}) + I_t \sin 3(\omega t + \tfrac{2\pi}{3}) \end{aligned}\right\} \tag{2}$$

Here, I_f is the amplitude of the fundamental current component, and I_t is the amplitude of the third-harmonic current component.

In the fundamental current component, there is a $2\pi/3$ phase difference between each of the three phases and the other two phases. In the third-harmonic current component, each of the three-phase currents has the same phase.

As the armature winding is supplied with fundamental and third-harmonic current components simultaneously, the neutral currents in this case are not zero and can be calculated as:

$$I_n = i_a + i_b + i_c = 3I_f \sin(3\omega t) \tag{3}$$

The voltage calculation equation is shown as (4).

$$v_y = R_{am} i_y + L_{am} \frac{di_y}{dt} \tag{4}$$

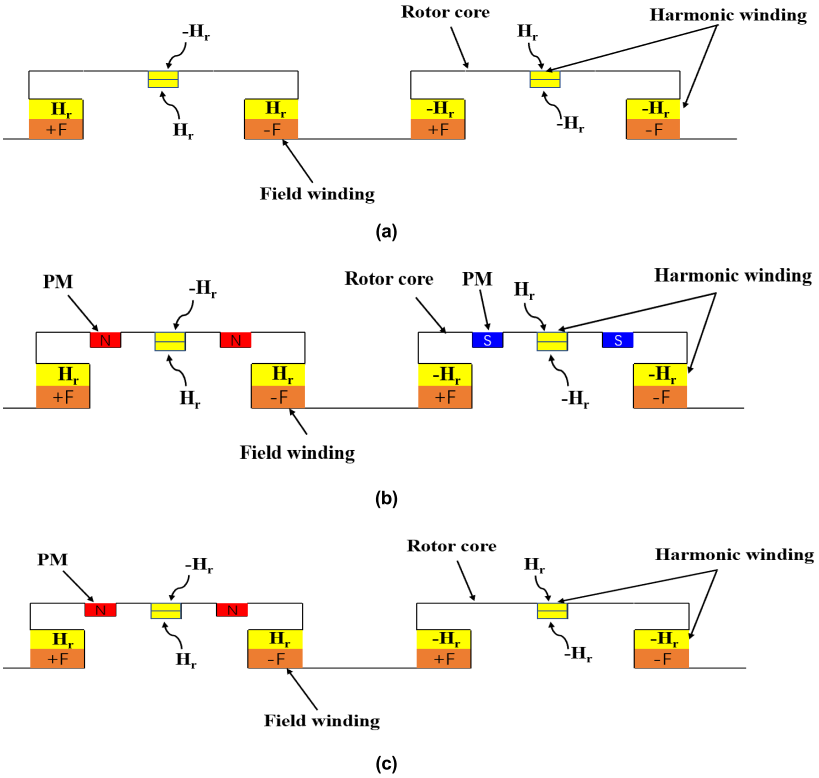

FIGURE 12. Simplified rotor structure of two poles for (a) BL-WRSM, (b) PM-BL-WRSM, and (c) CP-BL-WRSM.

From the above formula, $y\epsilon\{a, b, c\}$, i_y represents the inverter output current, v_y represents the inverter output voltage. L_{am} represents the inductance of the motor armature winding and R_{am} represents the resistance of the motor armature winding.

Machine models are provided with a composite shape of input armature currents, which are generated by the proposed inverter topology.

These currents generate 8-pole fundamental MMF and 24-pole third-harmonic MMF in the air gap. The resulting MMF is shown in equation (5).

$$\begin{aligned} F_a &= i_a N_p \sin\theta_e \\ F_b &= i_b N_p \sin(\theta_e - \frac{2\pi}{3}) \\ F_c &= i_c N_p \sin(\theta_e + \frac{2\pi}{3}) \end{aligned} \tag{5}$$

where N_p indicates the number of turns per phase, and $\theta_e = \omega_t + \theta_0$, ($\theta_e$ is used to denote the electrical angle whereas θ_0 indicates the initial rotor position).

The following formula is the net MMF (F_{abc}) generated by the provided three-phase input armature current:

$$F_{abc}(\theta_e, i_{abc}) = \frac{3I_f N_p \cos(\omega t - \theta_e)}{2} + I_t N_p \cos 3(\omega t + \theta_e) \tag{6}$$

The MMF generated in the air gap contains the fundamental component and the third-harmonic component. The fundamental component produces the main stator field, and the third-harmonic component produces a pulsating field in air gap.

Field winding and harmonic winding are installed on the motor rotor. The flux calculation equation of the rotor harmonic winding is shown in (7).

$$\lambda_{H_r} = \frac{N_{H_r} N_p (\frac{3}{2} I_f \cos(\omega t - \theta_e) + n I_t \cos(3\omega t + 3\theta_e))}{R_{ag}} \tag{7}$$

where R_{ag} is the air gap reluctance and N_{Hr} is the number of rotor harmonic turns.

The induced electromotive force in the rotor harmonic winding (EMF_{rhw}) of the machines is expressed by (8).

$$EMF_{rhw} = 6\frac{d\lambda_{H_r}}{dt} = \frac{18 N_{H_r} N_p I_t \omega \sin 3\,(2\omega t + \theta_0)}{R_{ag}} \tag{8}$$

where λ_{Hr} indicates the harmonic winding flux linkages of the rotor.

III. MACHINE TOPOLOGY

This paper uses an 8-pole, 42-slot (8p42s) machine to verify the proposed brushless WRSM topology. Fig. 9 shows the machine topology and the structures of the stator, and rotor.

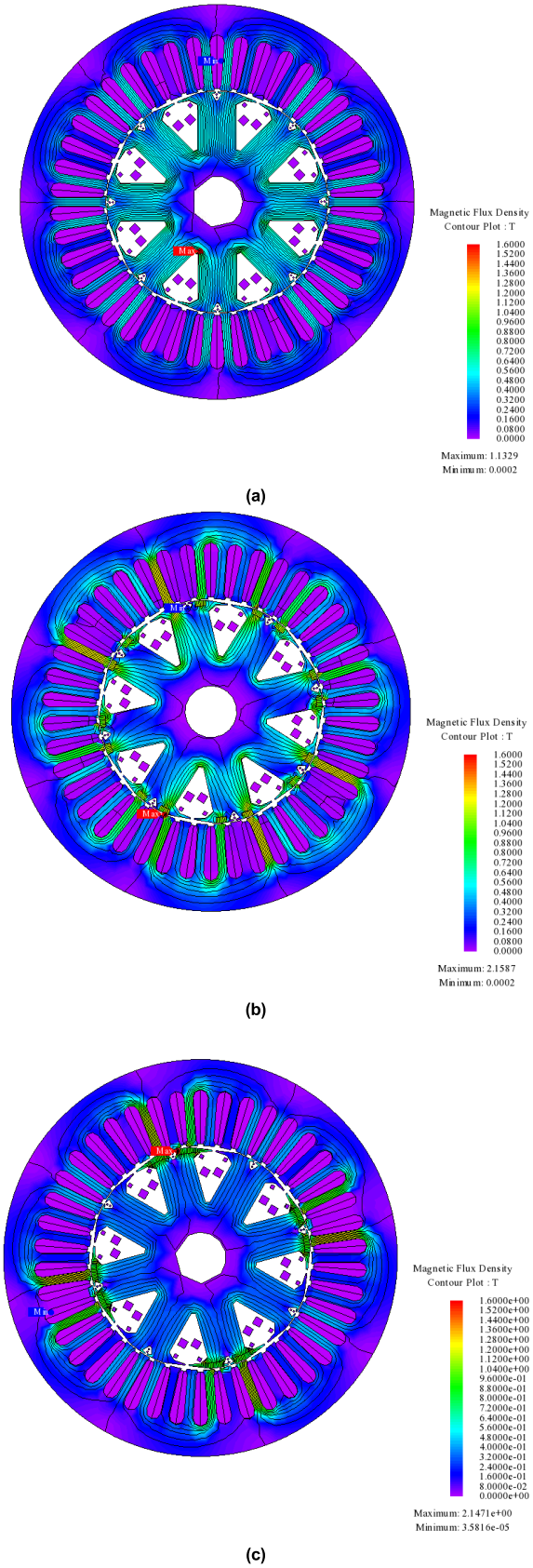

FIGURE 13. Flux density plots of (a) BL-WRSM, (b) PM-BL-WRSM, and (c) CP-BL-WRSM.

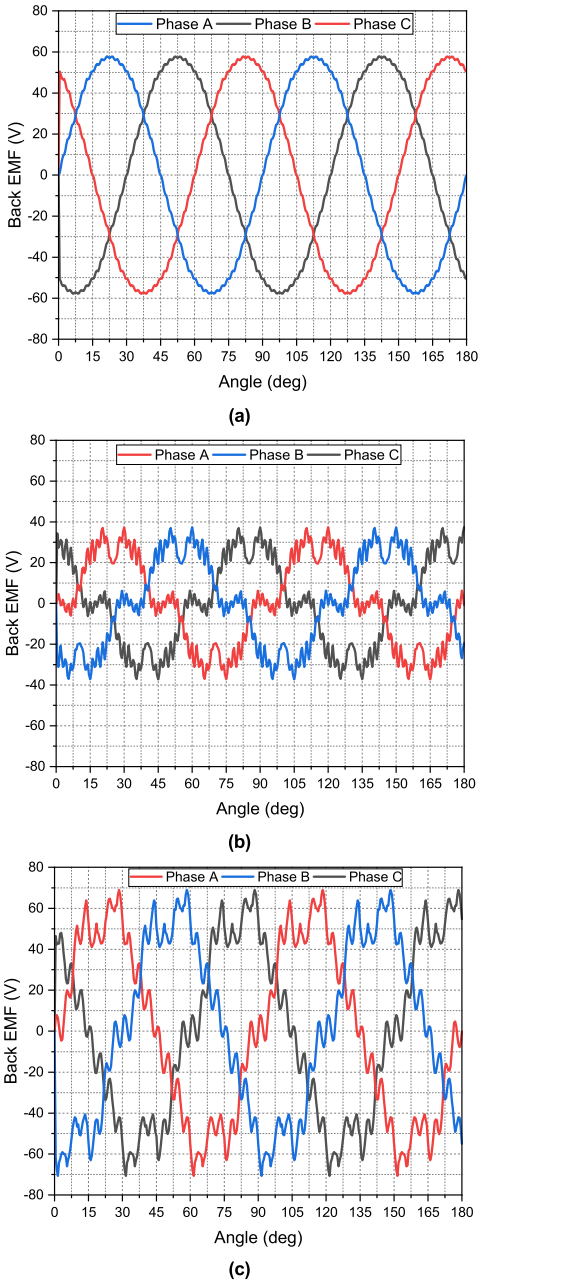

FIGURE 14. Back-EMF of (a) BL-WRSM, (b) PM-BL-WRSM, and (c) CP-BL-WRSM.

The three machine topologies use the same stator of 8 poles, and 42 slots as shown in Fig. 9(a). The rotor structures of the machines are shown in Fig 9 (b)-(d). The stator winding pattern used for the stator of machines is shown in Fig. 10. The winding factor and three-phase MMF of different harmonic numbers produced by the stator winding used in the three machine topologies are shown in Fig. 11(a) and (b). Table 1 shows the winding parameters used by this machine. The difference between the rotors used in the three machine topologies is the usage of PMs. PMs are inserted into all rotor

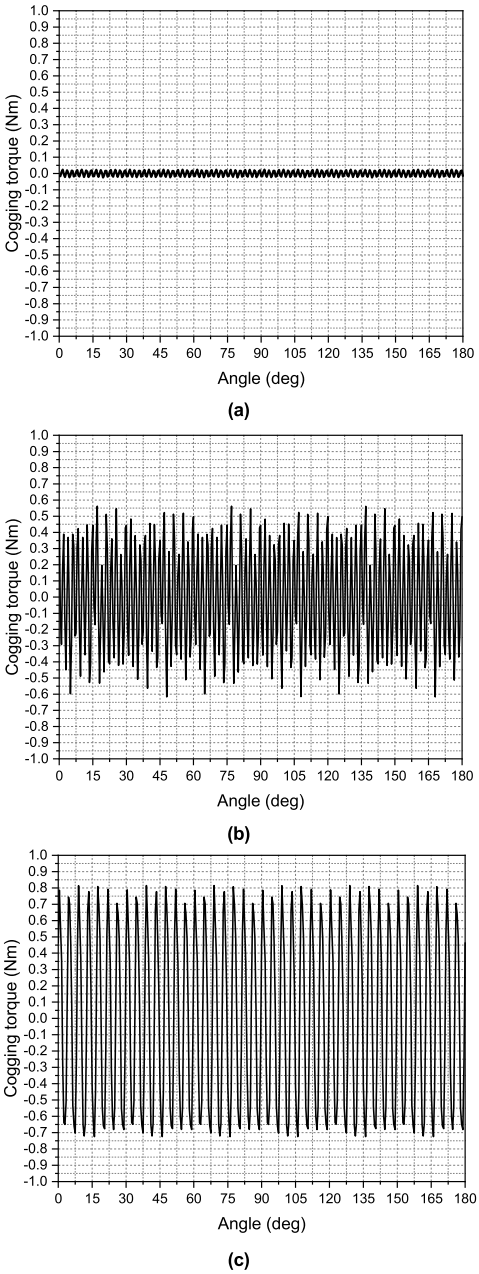

FIGURE 15. Cogging torque of (a) BL-WRSM, (b) PM-BL-WRSM, and (c) CP-BL-WRSM.

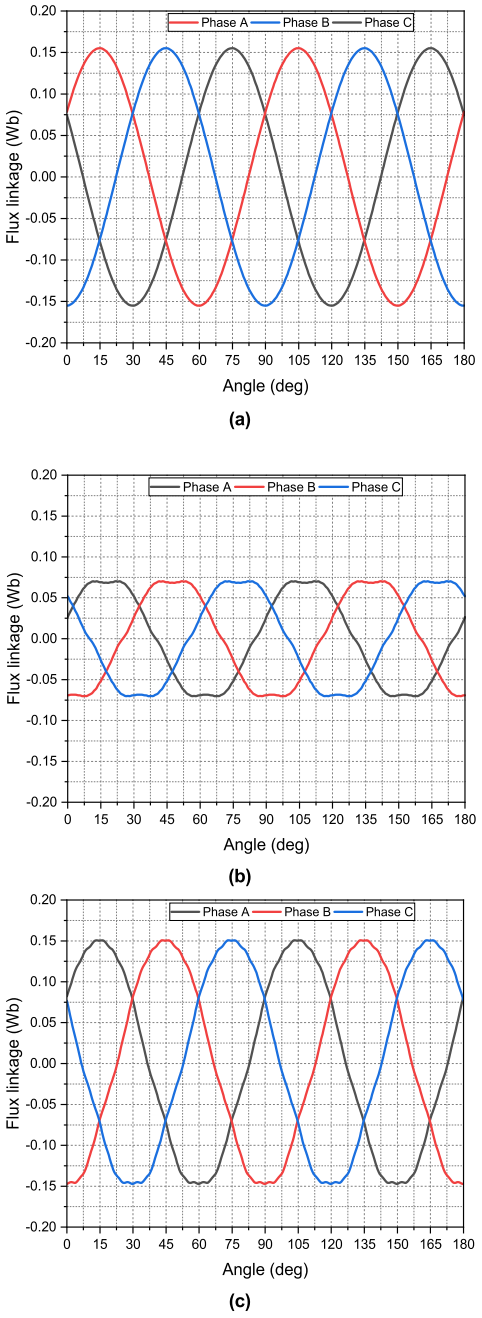

FIGURE 16. Flux density of (a). BL-WRSM, (b). PM-BL-WRSM, (c). CP-BL-WRSM.

poles of PM-BL-WRSM. However, PMs are inserted into the alternating rotor poles on CP-BL-WRSM. The conventional BL-WRSM does not employ any PMs for its rotor.

A. CONVENTIONAL BL-WRSM

The rotor used in BL-WRSM is an 8-pole rotor as shown in Fig. 9(b). The rotor of BL-WRSM has 8 main teeth to accommodate the rotor field winding, and each main tooth is further divided into two auxiliary teeth to accommodate the rotor's harmonic winding. Therefore, the machine rotor has 8 main teeth and 16 auxiliary teeth to accommodate 8 pole field winding and 24 poles of the harmonic winding. The configuration of the rotor winding is shown in Fig. 12(a).

B. PROPOSED PERMANENT-ASSISTED BL-WRSM (PM-BL-WRSM)

The difference between the PM-BL-WRSM and BL-WRSM rotors is that: 16 PMs are inserted into the rotor poles of the PM-BL-WRSM. That is, the rotor of the PM-BL-WRSM is a hybrid rotor with harmonic winding, field winding, and PMs. The hybrid rotor with windings and PMs helps the machine to start autonomously without outside help. The configuration of the rotor winding is shown in Fig. 12(b). The PM material used for PM-BL-WRSM is NdFeB (1.4 T), and the volume of the PMs is around 15.105 cm^3.

TABLE 2. Machine specifications.

Parameter	Units	BL-WRSM	PM-BL-WRSM	CP-BL-WRSM
Rated power	W	1	1	1
Frequency	Hz	60	60	60
Operating speed	rpm	900	900	900
Stator outer diameter	mm	88.5	88.5	88.5
Stator inner diameter	mm	50	50	50
Rotor diameter	mm	49.5	49.5	49.5
Rotor main/sub-teeth	mm	8/16	8/16	8/16
Air gap length	mm	0.5	0.5	0.5
Stack length	mm	80	80	80
Core material	-	50H1300	50H1300	50H1300
Magnet material	-	-	NdFeB (1.4T)	NdFeB (1.4T)
Magnet volume	cm^3	-	15.105	12.096

TABLE 3. Performance comparison in no-load condition by 2-D FEA.

Parameter	Units	BL-WRSM	PM-BL-WRSM	CP-BL-WRSM
Back-EMF	V rms	41.4727	21.5338	41.1369
Cogging torque	Nm	0.024	0.56	0.81

TABLE 4. Performance comparison in loaded condition by 2-D FEA.

Parameter	Units	BL-WRSM	PM-BL-WRSM	CP-BL-WRSM
Stator current	A rms	4	4	4
Starting torque	Nm	-0.037	4.34	6.39
Average output torque	Nm	2.78	6.07	6.88
Maximum output torque	Nm	4.37	7.15	8.03
Minimum output torque	Nm	3.12	5.44	5.63
Torque ripple	%	44.96%	27.82%	34.88%

C. PROPOSED CONSEQUENT-POLE BL-WRSM (CP-BL-WRSM)

The difference between the proposed CP-BL-WRSM and BL-WRSM rotors is that: 8 PMs are inserted into the rotor consequent poles of the CP-BL-WRSM. The difference between the proposed CP-BL-WRSM and PM-BL-WRSM rotors is the reduced number of permanent magnets inserted into the rotor consequent poles of the CP-BL-WRSM. The configuration of the rotor winding is shown in Fig. 12(c). The PM material used for the proposed CP-BL-WRSM is NdFeB (1.4 T), and the volume of PMs is around 12.096 cm^3.

The design parameters of the three machines are listed in Table 2.

IV. FINITE ELEMENT ANALYSIS

A. NO-LOAD ANALYSIS

As the no-load analysis of the machines will be helpful to describe the generation of torque ripple of the machines during motoring operation, JMAG-Designer is used to simulate the three machine topologies under no-load condition. A DC of 1 A is supplied to carry out the no-load analysis of the machines. These machines were operated at 900 rpm. The magnetic flux density plot is presented in Fig. 13(a)-(c), whereas Fig. 14(a)-(c) shows the back-EMF of the three machines. The cogging torque of BL-WRSM is 0.024 Nm, while the cogging torque of PM-BL-WRSM is 0.56 Nm. The cogging torque of CPH-BL-WRSM is 0.81 Nm. The cogging torque of the machines is shown in Fig. 15(a)-(c). Under no-load conditions, the flux linkage of the machine is presented in Fig. 16(a)-(c). The no-load analysis results of the machine models are presented in Table 3.

B. LOADED ANALYSIS

As the proposed machines are designed while considering the motoring operation only, the effectiveness of the proposed CP-BL-WRSM is verified by comparing the output torque results of the three machines. Except for the volume of the permanent magnet, the design parameters are the same for all three machines, including stack length, the length of air gap, number of rotor main and sub-teeth, coil diameters of stator and rotor, core material and magnet material, etc.

The armature winding current in the three machine topologies is 4 A. These three machines are running at a speed of 900 rpm. Within 0.8 seconds of simulation, both the torque and the field current reached at steady-state condition. The inverter supplies the composite armature current, which includes the fundamental current component and the third-harmonic current component. Among them, the fundamental current component produces the main stator magnetic field, and in the harmonic winding, the third-harmonic

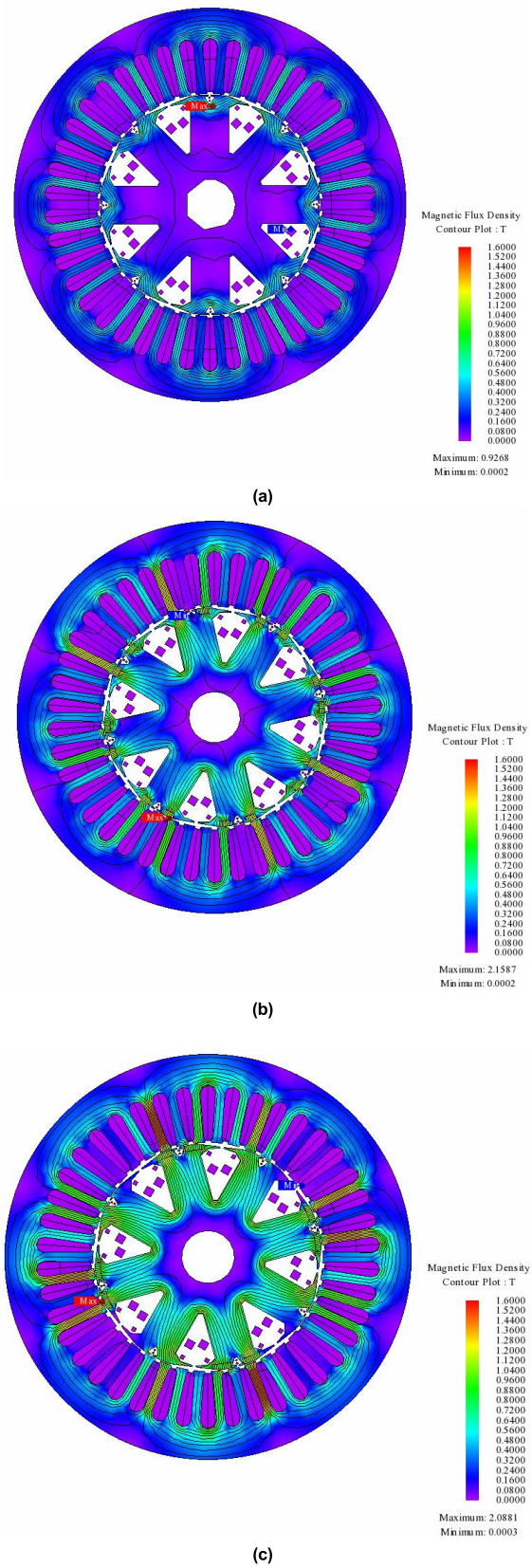

FIGURE 17. Flux density plot of (a) BL-WRSM, (b) PM-BL-WRSM, and (c) CP-BL-WRSM.

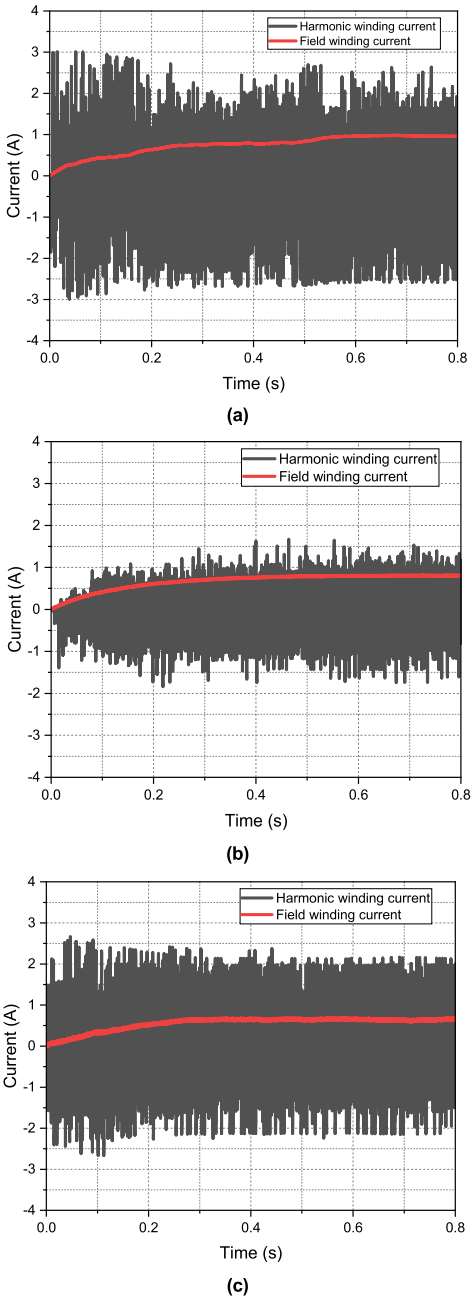

FIGURE 18. Induced harmonic currents and induced field currents of (a) BL-WRSM, (b) PM-BL-WRSM, and (c) CP-BL-WRSM.

current component induces a harmonic current. The harmonic current gets rectified by the diode rectifier injects DC into the field winding of the rotor to form a rotor magnetic field. The magnetic flux density plot of three machines is presented in Fig. 17(a)-(c). Figure 17(a)-(c) shows that the machine model runs below the saturation level of 1.6 T. The induced harmonic current and field current of the three machines is shown in Fig. 18(a)-(c). Fig. 18(a)-(c) shows that the average magnitude of the field current after the rectification of the BL-WRSM topology is 0.89A, and the

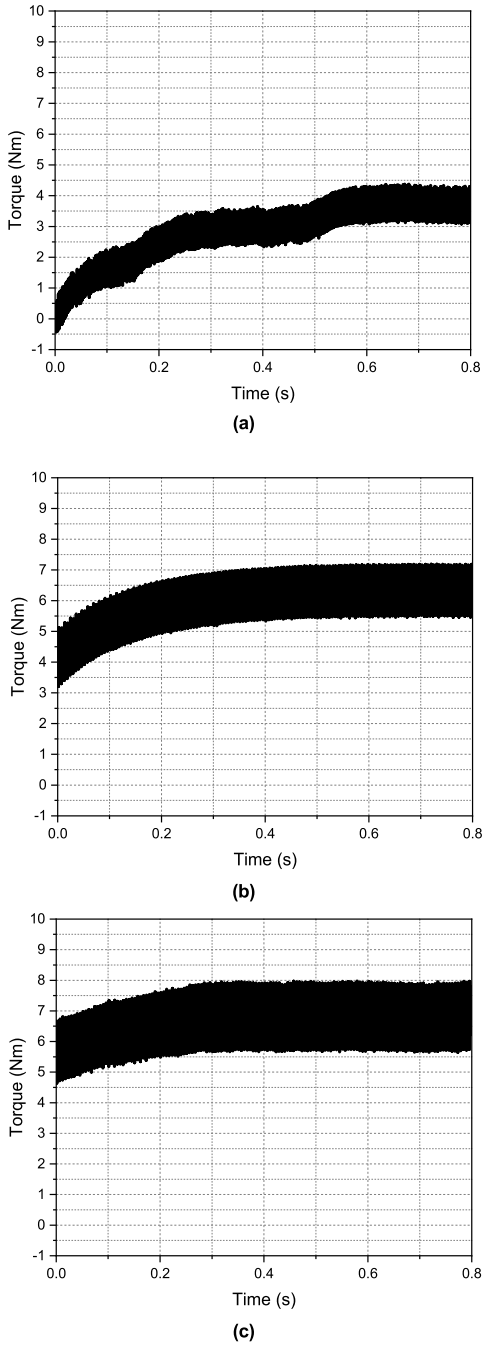

FIGURE 19. Output torque of (a) BL-WRSM, (b) PM-BL-WRSM, and (c) CP-BL-WRSM.

average magnitude of the field current after the rectification of the PM-BL-WRSM and CP-WRSM topology are 0.70 A and 0.57 A. As shown in Fig. 19(a)-(c), the average torque generated by the BL-WRSM topology is 2.78 Nm. The average torque generated by the PM-BL-WRSM topology is 6.07 Nm, which is 59.59% higher than the average output torque range of BL-WRSM and 13.34% higher than the average output torque of PM-BL-WRSM. The average torque generated by the CP-BL-WRSM, is 6.88 Nm. The starting torque of BL-WRSM is around-0.037 Nm. However, the starting torque of PM-BL-WRSM and CP-BL-WRSM has been greatly increased. The starting torques of the two machines are 4.34 Nm, and 6.39 Nm, respectively. The maximum output torque of BL-WRSM topology is 4.37 Nm, while the maximum output torque of PM-BL-WRSM is 7.15 Nm, and CP-BL-WRSM topology is 8.03 Nm. The torque ripples of BL-WRSM, PM-BL-WRSM and CP-BL-WRSM are 44.96%, 27.82%, and 34.88%. The torque ripple of the CP-BL-WRSM is 10.08% lower than that of the BL-WRSM. Table 4 summarizes the performance comparison of the three machine topologies for average output torque, starting torque, maximum torque, and torque ripple.

V. CONCLUSION

In this paper, the PM-BL-WRSM and CP-BL-WRSM topologies are proposed. The main target of these topologies is to achieve better torque characteristics on the third-harmonic field excitation technique for the conventional BL-WRSM topology. Moreover, CP-BL-WRSM can obtain better performance than PM-BL-WRSM while using less permanent magnet volume. In this proposed topology, a PM is installed on the alternative rotor poles. The operation and performance of the three machine topologies were verified using 2-D FEA. It can be seen from the comparison that the proposed CP-BL-WRSM topology performs well as compared to the other two machines in terms of torque characteristic such as output maximum, minimum, average, and starting torques. The volume of the PMs used in the proposed CP-BL-WRSM machine topology is 12.096 cm^3. The CH-BL-WRSM uses 3.009 cm^3 less volume of PMs as compared to PM-BL-WRSM.

REFERENCES

[1] Q. Ali, T. A. Lipo, and B.-I. Kwon, "Design and analysis of a novel brushless wound rotor synchronous machine," *IEEE Trans. Magn.*, vol. 51, no. 11, pp. 1–4, Nov. 2015.

[2] Q. Ali, S. S. H. Bukhari, and S. Atiq, "Variable-speed, sub-harmonically excited BL-WRSM avoiding unbalanced radial force," *Electr. Eng.*, vol. 101, no. 1, pp. 251–257, Apr. 2019.

[3] G. J. Sirewal, M. Ayub, S. Atiq, and B.-I. Kwon, "Analysis of a brushless wound rotor synchronous machine employing a stator harmonic winding," *IEEE Access*, vol. 8, pp. 151392–151402, 2020.

[4] S. S. H. Bukhari, H. Ahmad, F. Akhtar, and J. Ro, "Brushless field excitation method for wound-rotor synchronous machines," *Int. Trans. Elect. Energy Syst.*, vol. 31, no. 8, p. e12961, 2021.

[5] M. Ayub, S. S. H. Bukhari, G. Jawad, A. Arif, and B. I. Kwon, "Utilization of reluctance torque for improvement of the starting and average torques of a brushless wound field synchronous machine," *Elect. Eng.*, vol. 103, pp. 1–7, Oct. 2021.

[6] M. Ayub, S. Atiq, Q. Ali, A. Hussain, and B.-I. Kwon, "Dual-mode wound rotor synchronous machine for variable speed applications," *IEEE Access*, vol. 8, pp. 115812–115822, 2020.

[7] M. Ayub, A. Hussain, G. Jawad, and B.-I. Kwon, "Brushless operation of a wound-field synchronous machine using a novel winding scheme," *IEEE Trans. Magn.*, vol. 55, no. 6, pp. 1–4, Jun. 2019.

[8] L. Sun, X. Gao, F. Yao, Q. An, and T. Lipo, "A new type of harmonic current excited brushless synchronous machine based on an open winding pattern," in *Proc. IEEE Energy Convers. Congr. Expo. (ECCE)*, Pittsburgh, PA, USA, Sep. 2014, pp. 2366–2373.

[9] F. Yao, Q. An, L. Sun, and T. A. Lipo, "Performance investigation of a brushless synchronous machine with additional harmonic field windings," *IEEE Trans. Ind. Electron.*, vol. 63, no. 11, pp. 6756–6766, Nov. 2016.

[10] F. Yao, Q. An, X. Gao, L. Sun, and T. A. Lipo, "Principle of operation and performance of a synchronous machine employing a new harmonic excitation scheme," *IEEE Trans. Ind. Appl.*, vol. 51, no. 5, pp. 3890–3898, Sep./Oct. 2015.
[11] Q. An, X. Gao, F. Yao, L. Sun, and T. Lipo, "The structure optimization of novel harmonic current excited brushless synchronous machines based on open winding pattern," in *Proc. IEEE Energy Convers. Congr. Exposit. (ECCE)*, Pittsburgh, PA, USA, Sep. 2014, pp. 1754–1761.
[12] F. Yao, Q. An, L. Sun, M. S. Illindala, and T. A. Lipo, "Optimization design of stator harmonic windings in brushless synchronous machine excited with double-harmonic-windings," in *Proc. Int. Energy Sustainability Conf. (IESC)*, Farmingdale, NY, USA, Oct. 2017, pp. 1–6.
[13] G. Jawad, Q. Ali, T. A. Lipo, and B. I. Kwon, "Novel brushless wound rotor synchronous machine with zero-sequence third-harmonic field excitation," *IEEE Trans. Magn.*, vol. 52, no. 7, pp. 1–4, Jul. 2016.
[14] M. Ayub, G. Jawad, S. S. H. Bukhari, and B.-I. Kwon, "Brushless wound rotor synchronous machine with third harmonic field excitation," *Electr. Eng.*, vol. 102, no. 1, pp. 259–265, Mar. 2020.
[15] S. S. H. Bukhari, G. J. Sirewal, M. Ayub, and J. Ro, "A new small-scale self-excited wound rotor synchronous motor topology," *IEEE Trans. Magn.*, vol. 57, no. 2, pp. 1–5, Feb. 2021.
[16] S. S. H. Bukhari, H. Ahmad, F. Akhtar, and J. Ro, "Brushless field excitation method for wound-rotor synchronous machines," *Int. Trans. Elect. Energy Syst.*, vol. 31, no. 8, p. e12961, 2021.
[17] M. Ayub, S. S. H. Bukhari, and B.-I. Kwon, "Brushless wound field synchronous machine with third-harmonic field excitation using a single inverter," *Electr. Eng.*, vol. 101, no. 1, pp. 165–173, Apr. 2019.
[18] S. S. H. Bukhari, G. J. Sirewal, F. A. Chachar, and J. Ro, "Dual-inverter-controlled brushless operation of wound rotor synchronous machines based on an open-winding pattern," *Energies*, vol. 13, no. 9, p. 2205, May 2020.
[19] S. S. H. Bukhari, G. J. Sirewal, S. Madanzadeh, and J. Ro, "Cost-effective single-inverter-controlled brushless technique for wound rotor synchronous machines," *IEEE Access*, vol. 8, pp. 204804–204815, 2020.
[20] S. S. H. Bukhari, A. A. Memon, S. Madanzadeh, G. J. Sirewal, J. Doval-Gandoy, and J. Ro, "Novel single inverter-controlled brushless wound field synchronous machine topology," *Mathematics*, vol. 9, no. 15, p. 1739, Jul. 2021.
[21] S. S. H. Bukhari, H. Ahmad, G. J. Sirewal, and J. Ro, "Simplified brushless wound field synchronous machine topology based on a three-phase rectifier," *IEEE Access*, vol. 9, pp. 8637–8648, 2021.
[22] Q. Ali, S. Atiq, T. A. Lipo, and B. I. Kwon, "PM assisted, brushless wound rotor synchronous machine," *J. Magn.*, vol. 21, no. 3, pp. 399–404, Nov. 2016.
[23] S.-W. Hwang, J.-H. Sim, J.-P. Hong, and J.-Y. Lee, "Torque improvement of wound field synchronous motor for electric vehicle by PM-assist," *IEEE Trans. Ind. Appl.*, vol. 54, no. 4, pp. 3252–3259, Jul. 2018.
[24] A. Hussain, S. Atiq, and B.-I. Kwon, "Consequent-pole hybrid brushless wound-rotor synchronous machine," *IEEE Trans. Magn.*, vol. 54, no. 11, pp. 1–5, Nov. 2018.
[25] M. Ayub, G. Jawad, and B.-I. Kwon, "Consequent-pole hybrid excitation brushless wound field synchronous machine with fractional slot concentrated winding," *IEEE Trans. Magn.*, vol. 55, no. 7, pp. 1–5, Jul. 2019.
[26] D. Li, R. Qu, J. Li, and W. Xu, "Consequent-pole toroidal-winding outer-rotor Vernier permanent-magnet machines," *IEEE Trans. Ind. Appl.*, vol. 51, no. 6, pp. 4470–4481, Nov./Dec. 2015.
[27] S.-U. Chung, J.-W. Kim, Y.-D. Chun, B.-C. Woo, and D.-K. Hong, "Fractional slot concentrated winding PMSM with consequent pole rotor for a low-speed direct drive: Reduction of rare earth permanent magnet," *IEEE Trans. Energy Convers.*, vol. 30, no. 1, pp. 103–109, Mar. 2015.